

# Maxwell-Bloch modeling of an x-ray pulse amplification in a 1D photonic crystal

O. Peyrusse\*

*Aix-Marseille Univ., CNRS UMR 7345, PIIM Marseille, France*

P. Jonnard, J.-M. André

*Sorbonne Université, Faculté des Sciences et Ingénierie, UMR CNRS,*

*Laboratoire de Chimie Physique - Matière et Rayonnement,*

*4 Place Jussieu, F-75252 Paris Cedex 05, France*

(Dated: December 22, 2024)

## Abstract

We present an implementation of the Maxwell-Bloch (MB) formalism for the study of x-ray emission dynamics from periodic multilayer materials whether they are artificial or natural. The treatment is based on a direct Finite-Difference-Time-Domain (FDTD) solution of Maxwell equations combined with Bloch equations incorporating a random spontaneous emission noise. Besides periodicity of the material, the treatment distinguishes between two kinds of layers, those being active (or resonant) and those being off-resonance. The numerical model is applied to the problem of  $K\alpha$  emission in multilayer materials where the population inversion could be created by fast inner-shell photoionization by an x-ray free-electron-laser (XFEL). Specificities of the resulting amplified fluorescence in conditions of Bragg diffraction is illustrated by numerical simulations. The corresponding pulses could be used for specific investigations of non-linear interaction of x-rays with matter.

PACS numbers:

---

\*Electronic address: [olivier.peyrusse@univ-amu.fr](mailto:olivier.peyrusse@univ-amu.fr)

## I. INTRODUCTION

Non-linear optical devices (NLO) have been a vivid subject of study for their numerous applications. Within the domain of x-ray quantum optics [1, 2], the field of non-linear x-ray (NLX-ray) devices is much less explored since, compared with the optical range, the control of x-rays is more difficult. The simplest NLX-ray device is an ensemble of 2,3-level atoms for which different studies of pulse propagation and of several non-linear effects have been reported (see for instance [3]). Another typical NLX-ray devices are multilayer materials which are used in x-ray optics. Short and ultra-intense x-ray sources such as x-ray free electron lasers (XFELs) are pushing the boundaries of the response to x-rays in such devices. Besides this, it has been proved that XFEL sources have the potential to create large population inversions in gases [4], clusters [5], solids [6–8] and liquids [9], resulting in the creation of an x-ray amplifying medium. These approaches based on lasing in atomic media have an important potential to obtain useful short and coherent x-ray pulses. Indeed, high-quality short pulses going beyond the inherent defaults of SASE XFEL pulses (of spiky and chaotic nature) are a prerequisite for future investigations concerning x-ray quantum optics, x-ray scattering, precision spectroscopy or pump-probe experiments requiring a coherent probe. Compared with conventional lasers, these approaches suffer from the lack of a resonator to extract most of the energy stored in an inverted medium. In other words, there remains the problem of realizing x-ray feedback to achieve laser oscillation in the x-ray range. Hence a work going in that direction has recently been reported [10]. In this reported work a classical multipass meter-sized laser cavity has been set up. The x-ray lasing medium being a liquid jet pumped by an XFEL. Besides this, within the context of XFEL excitation and to extract energy stored in an inverted medium, the idea of using the phenomenon of collective spontaneous decay or superradiance (named also superfluorescence) has been discussed and explored [11] but in the visible range. Independently, it has been suggested that a laser action in the x-ray range can be provided by Bragg reflection inside a natural crystal or inside an artificial multilayer material [12–14]. Note that in the first case, Bragg condition is constrained by the crystal periodicity.

The goal of this paper is to study numerically x-ray feedback under Bragg conditions as well as pulse propagation in 1D photonic crystals in which a population inversion has been initiated by some external source. Here we go beyond a description where the multilayer is

simply described by the complex refractive index of each layer [14]. Even when the complex part of the refractive index is negative (i.e. amplifying), such a description is basically linear and corresponds to the linear phase of the interaction of an x-ray pulse with the material. Note that this remark concerns the *active* layers only. *Passive* layers, for which no resonant response is expected, can still be described by a complex refractive index. This defines the specificity of our description which mixes a non-linear treatment and a linear treatment, i.e. more precisely using a Maxwell-Bloch (MB) formalism or a standard formalism, depending on the kind of layer (active or passive).

In this paper we consider a large number of photons in the radiation modes. As a consequence, quantum fluctuations are neglected and the electromagnetic (EM) field is described by Maxwell equations. In the absence of an external source, one shortcoming of the MB description is that there is no mechanism for spontaneous emission. It is well-known that this problem can be overcome by adding a phenomenological fluctuating polarization source that simulates spontaneous emission. Compared with many calculations of x-ray lasing in gas or plasmas (see for instance Refs [15–18]) short spatial scales involved in this multilayer context, do not permit the use of the *slowly varying envelope approximation* so that basic Maxwell equations have to be solved directly. This is done here using the so-called Finite-Difference-Time-Domain (FDTD) method [19]. Furthermore, in this multilayer (or 1D photonic crystal) context, we consider a 1D plane geometry. Also, we consider only two levels resonantly coupled to the EM field in the MB system. Other levels are taken into account through relaxation and source terms in the equations governing populations of these two levels.

In the following, we present the physical model used here (Sec. II), underlining the specific choices made for considering 1D photonic crystals in the x-ray range. Then, we turn to a discussion of simulation results in Sec. III. Physical situations considered here evolve gradually from very formal situations to situations close to actual experimental conditions. So, after some considerations on the validity of the implementation of the model, we consider in detail the problem of an x-ray pulse propagation in a particular stack of bi-layers (Mg/Co) in which a population inversion is supposed. After this, one considers the self-emission of such a stack, i.e. as initiated by spontaneous emission. Finally, we turn to situations where an XFEL source is used for pumping (i.e. for creating the population inversion) either a multilayer (such as a bi-layer (Mg/Co) stack) or a simple Si crystal. Section IV summarizes

these results.

## II. THEORETICAL APPROACH

### A. Basic equations

As said in the introduction, the medium considered here consists of alternating *active* and *passive* materials with a given periodicity. *Active* in the sense of resonantly coupled with the EM field at some pulsation  $\omega_o$  and *passive* if there is no resonant coupling. The two first basic equations of our approach are the Faraday and the Ampere's laws, respectively written in the form (SI units)

$$\vec{\nabla} \times \vec{E} = -\partial_t \vec{B} \quad (1)$$

$$\frac{1}{\mu_o} \vec{\nabla} \times \vec{B} = \epsilon_o \epsilon_r \partial_t \vec{E} + \vec{j} \quad (2)$$

$\vec{E}$ ,  $\vec{B}$  are the electric and the magnetic fields (real quantities), respectively.  $\epsilon_o$ ,  $\mu_o$  are the vacuum permittivity and permeability, respectively.  $\epsilon_r$  is the relative permittivity (here time-independent) and  $\vec{j}$  is the local current induced by the EM field. In a linear material, i.e. here in a *passive* layer,  $\vec{j} = \sigma \vec{E}$  where  $\sigma$  is the electric conductivity. At pulsation  $\omega_o$ , adiabatic properties of the material (in the sense of an instantaneous response to the applied field) are included in the *real* quantities  $\epsilon_r$  et  $\sigma$ . If the material is described by a complex refractive index of the form (as in current data tables [20, 21]),

$$n = (1 - \delta) - i\beta,$$

there is an equivalence between the conductivity approach and the refractive index in the sense that

$$\epsilon_r = (1 - \delta)^2 - \beta^2$$

$$\sigma = 2(1 - \delta)\beta\omega_o\epsilon_o$$

In a so-called *active* medium such as the so-called *active* layers, one has  $\vec{j} = \partial_t \vec{\mathcal{P}}$  where  $\vec{\mathcal{P}}$  is the macroscopic polarization. Considering two levels coupled by the EM field, the

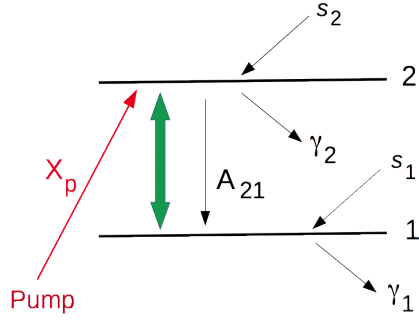


FIG. 1: (Color online) Level scheme with the associated source or loss rates. The big line with 2 arrows represents the Bloch-Maxwell coupling.

macroscopic polarization is defined as the trace of the operator  $N\rho\vec{d}$  where  $N$  is the density of polarizable atoms,  $\vec{d}$  is the atomic dipole and  $\rho$  is the density matrix. Hence

$$\vec{\mathcal{P}} = 2N\text{Re}[\rho_{21}]\vec{d} \quad (3)$$

The non-diagonal matrix element of the density matrix  $\rho_{21}$  is a complex number as the diagonal elements  $\rho_{11}$ ,  $\rho_{22}$  are real quantities. These matrix elements are obtained from the following evolution of the density matrix (Liouville equation)  $i\hbar\partial_t = [H, \rho] +$  relaxation/source terms. Here, assuming a polarization along axis Ox, the hamiltonian  $H$  has the form  $H = \begin{pmatrix} \epsilon_1 & -dE_x \\ -dE_x & \epsilon_2 \end{pmatrix}$  where both  $E_x$  and  $d = \langle 1|\vec{d}|2 \rangle$  are real quantities.  $\epsilon_{1,2}$  are the energies of the coupled levels. Hereafter,  $\hbar\omega_o = \epsilon_2 - \epsilon_1$ . Level scheme of the problem is depicted in Fig. 1.

In a more or less hot medium,  $\gamma_1$ ,  $\gamma_2$  are the rates (in  $\text{s}^{-1}$ ) of the collisional and radiative processes which couple states together, except absorption, stimulated emission and spontaneous emission.  $A_{21}$  is the spontaneous emission rate. Here  $s_1$ ,  $s_2$  are the possible population fluxes due to the processes involving other levels in the system. We define  $\gamma_{\perp} = \frac{1}{2}(\gamma_1 + \gamma_2) + \gamma_{\phi}$  so that  $1/\gamma_{\perp}$  can be seen as the life time of the coherent superposition of states  $|1 \rangle$  and  $|2 \rangle$ . In principle,  $\gamma_{\phi}$  is supposed to be the rate of events perturbing the wave-function without inducing a decay of eigenstates. Hereafter, we called populations of states 1 and 2 the macroscopic quantities  $N_1 = N\rho_{11}$ ,  $N_2 = N\rho_{22}$ , respectively.

In an active layer, the set of equations to be solved locally for the populations  $N_1$ ,  $N_2$  and

for  $P = N\rho_{21}$ , is then,

$$\partial_t N_1 = -\frac{2}{\hbar}dE_x\text{Im}[P] + s_1 - \gamma_1 N_1 + A_{21}N_2 \quad (4)$$

$$\partial_t N_2 = \frac{2}{\hbar}dE_x\text{Im}[P] + s_2 - \gamma_2 N_2 - A_{21}N_2 + X_p \quad (5)$$

$$\partial_t P = -i\omega_o P - \gamma_{\perp} P - i(N_2 - N_1)dE_x + S \quad (6)$$

where we added in Eq. (5), a pump source term  $X_p$ .  $S$  is a phenomenological random source modeling the spontaneous emission. In the absence of external incoming radiation,  $S$  acts as an energy seed for energy injection in the system. Eqs.(1)-(6) correspond to our set of Bloch-Maxwell equations where Eqs. (4)-(6) concern the active layers only. In the literature, the name of Bloch-Maxwell [22], or sometimes Maxwell-Schrödinger [15], is often given to the coupling of complex slowly varying *envelopes* of the EM field with the Bloch equations for the density matrix. Here, there is no approximation concerning the field variation both in space and time.

## B. Wave equations in a 1D photonic medium at oblique incidence

A sketch of the physical problem is given in Figure 2. The medium is made of a periodic stack of different materials (at least two different materials). One is the active material (i.e. described by the MB equations), the other(s) is(are) the passive (or linear) material(s), i.e. described by complex refractive indices.

$(\vec{k}, \vec{E}, \vec{B})$  represent a plane-wave propagating in the material under the angle  $\theta_{\perp}$ . Hereafter we make use of  $\theta_{\perp}$  which is the angle with respect to a direction *perpendicular* to surface  $xy$  while it may be more convenient to use  $\theta_{//} = \frac{\pi}{2} - \theta_{\perp}$ . In this geometry, Faraday's law (Eq. (1)) reads,

$$\partial_z E_x = -\partial_t B_y \quad (7)$$

$$\partial_y E_x = \partial_t B_z \quad (8)$$

while the Ampere's law (Eq. (2)) reads

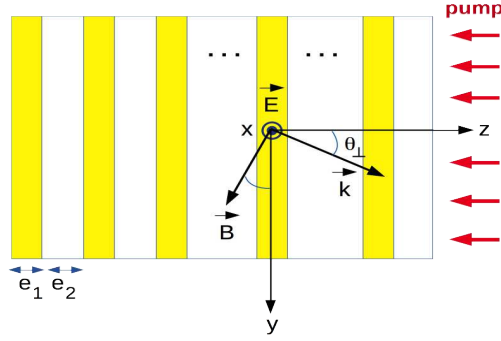


FIG. 2: (Color online) Sketch of a stack of bilayers made of one *active* element (yellow) and of one *passive* element. On one side the stack is submitted to a source of excitation (the pump). Propagation of the emerging radiation is described by Maxwell equations at some wavelength (which is resonant for the active layers). In active layers, response is described by the Bloch equations while in passive layers, response is given by the refractive index.

$$-\partial_z B_y + \partial_y B_z = \frac{\epsilon_r}{c^2} \partial_t E_x + \mu_o j_x \quad (9)$$

where  $j_x = \sigma E_x$  in a *passive* layer. In an *active* layer,  $\epsilon_r = 1$  and  $j_x = \partial_t \mathcal{P}_x$ ,  $\mathcal{P}_x$  being deduced from Eq. (3), i.e.  $\mathcal{P}_x = 2d\text{Re}[P]$ . Translating (7), (8), (9) from the time-domain to the frequency-domain gives three equations in which  $E_x$  has the behavior  $E_x \sim \exp(i\omega_o t \pm iky \sin \theta_\perp)$ . Eliminating  $B_z$  and going back to the time domain ( $i\omega_o \rightarrow \partial_t$ ) finally gives the following two equations governing the behavior of a plane-wave for an arbitrary oblique incidence in the multilayer material,

$$\partial_z E_x = -\partial_t B_y \quad (10)$$

$$\partial_z B_y = \frac{1}{c^2} (\epsilon_r - \sin^2 \theta_\perp) \partial_t E_x + \mu_o j_x. \quad (11)$$

To solve these equations, one uses the usual FDTD method [19] namely a second-order central difference scheme introduced by Yee [23]. Yee's scheme consists in writing the central differences of  $E_x$  and  $B_y$ , shifted in space by half a cell and in time by half a time step. In our implementation,  $B$  is evaluated at the edge of each cell while  $E$  is evaluated at the center. Accordingly, proper boundary conditions for  $B$  have to be applied on each side of the multilayer. Considering that the two external layers (on both sides) correspond to the

vacuum (refractive index  $n = 1$ ), and in order to remove reflections from these boundaries, we used second-order Absorbing Boundary Conditions (ABC) [24]. Together with  $E_x$ , the quantities  $N_1$ ,  $N_2$  and  $P$  are cell-centered and are advanced in time using a Crank-Nicolson scheme.

Concerning the sampling in space, typically at least 20 steps per wavelength are necessary. This involves a subdivision of each layer in much smaller layers of thicknesses  $\Delta z$ . Accordingly, the sampling in time is governed by the Courant limit. More precisely, an inspection of Eq. (11) shows that the front phase velocity is  $c/\sqrt{\epsilon_r - \sin^2 \theta_\perp}$ . Then the time-step must be such that

$$\Delta t \leq \frac{\Delta z}{c} \sqrt{\epsilon_r - \sin^2 \theta_\perp}.$$

### C. Incident source - Spontaneous emission

For some applications, it may be useful to consider the seeding of the multilayer by some incident external polarized X-ray pulse. Practically, this can be an external source of X-rays generated independently. In order to follow an X-ray pulse propagating in one specific direction, the positive z-direction for instance (see Fig. 2), this source has to be properly implemented. As usual in FDTD simulations, this is accomplished using a total-field/scattered-field (TFSF) boundary [25] at the point where the source(s) is(are) put. Most often this source is placed in the left vacuum cell of our simulation domain. More precisely, one defines both an incident electric field  $E^{inc}$  and an incident magnetic field  $B^{inc} = \cos \theta_\perp \sqrt{\epsilon_r} E^{inc}$  ( $\epsilon_r = 1$  in the vacuum). At the location of the source, according to the TFSF method,  $E$  must be replaced by  $E - E^{inc}$  in the discretized evolution of the B field while  $B$  must be replaced by  $B + B^{inc}$  in the discretized evolution of the E field.

Independently of any external source, the source of spontaneous emission in Eq. (6) (the term  $S$ ) can be modeled as a Gaussian white noise following the guidelines of Ref. [16], an approach followed later by others [17, 18]. The interest of this approach is that it provides the correct spectral behavior for the field [16]. Here, one starts from the simplified (local) system (see Eq. (11) and Eq. (6)) coupling the electric field and  $P = N\rho_{21}$

$$\frac{dE}{dt} = \alpha \text{Re}\left[\frac{dP}{dt}\right] \quad (\alpha = -2\mu_o c^2 d) \quad (12)$$

$$\frac{dP}{dt} = -i\omega_o P - \gamma P + S \quad (13)$$

where the noise source  $S$  (complex) has the correlation function  $\langle S^*(t')S(t) \rangle = F\delta(t' - t)$ . The notation  $\langle \dots \rangle$  is used to represent the statistical ensemble averaging and  $F$  is a constant defined by the following arguments. From the density of the electric field  $\frac{\epsilon_o}{2}E^2$ , one defines an average power density  $W$  which must be equal to the power emitted by spontaneous emission (in one direction) so that,

$$W = \frac{d}{dt}\left(\frac{\epsilon_o}{2}\langle E^2 \rangle\right) = \frac{1}{4\pi}N_2A_{21}\hbar\omega_o \quad (14)$$

From the formal solution of Eq. (12),  $E(t) = \alpha \int_{-\infty}^t \text{Re}\left[\frac{dP(t')}{dt'}\right]dt'$ , one gets

$$W = \epsilon_o \langle E \frac{dE}{dt} \rangle = \alpha^2 \epsilon_o \int_{-\infty}^t \langle \text{Re}\left[\frac{dP(t')}{dt'}\right] \text{Re}\left[\frac{dP(t)}{dt}\right] \rangle dt'. \text{ Using (13), } W \text{ becomes,}$$

$$W = \frac{\epsilon_o}{4}\alpha^2 \int_{-\infty}^t \left( \left\langle \frac{dP^*(t')}{dt'} \frac{dP(t)}{dt} \right\rangle + \left\langle \frac{dP(t')}{dt'} \frac{dP^*(t)}{dt} \right\rangle \right) dt'. \quad (15)$$

From the formal solution of Eq. (13),  $P(t) = \int_{-\infty}^t S(t')e^{-i\omega_o(t-t')}e^{-\gamma(t-t')}dt'$ , it is easy to calculate quantities  $\langle \dots \rangle$ , so that after averaging over one period, calculation of the integrals in (15) gives (since  $\omega_o \gg \gamma$ )  $W = \frac{\epsilon_o}{4}\alpha^2 \frac{F}{2} \frac{\omega_o^2}{\gamma^2}$ . Then from relation (14), one gets

$$F(z, t) = \frac{2A_{21}\hbar\omega_o N_2(z, t)}{\alpha^2 \pi \epsilon_o} \frac{\gamma^2}{\omega_o^2}. \quad (16)$$

Practically, over a time step  $\Delta t$ , the noise source term  $S$  in Eq. (6) is a random complex number  $u + it$  distributed according to the law  $\frac{1}{\pi\sigma_S^2} \exp -(u^2 + t^2)/\sigma_S^2$  with  $\sigma_S = \sqrt{F\Delta t}$ .

### III. SIMULATIONS RESULTS

A numerical code based on the model described above has been built. The *active* materials considered in this article are K-shell photoionized magnesium or silicium. In magnesium, according to the level scheme depicted in Fig. 1, level 2 stands for  $1s 2s^2 2p^6 [3s^2]$  and level 1 stands for  $1s^2 2s^2 2p^5 [3s^2]$ . In silicium, level 2 stands for  $1s 2s^2 2p^6 [3s^2 3p^2]$  and level 1 stands for  $1s^2 2s^2 2p^5 [3s^2 3p^2]$ . Compared with neutral atoms, outer electrons in solid Mg or

Si (denoted by [...]) are more or less delocalized. In what follows, we either set populations 2 and 1 (likewise the density of inversion) or we explicitly consider a time-dependent pumping. In this last case, initial atoms (in the state  $|0\rangle \equiv 1s^2 2s^2 2p^6 [3s^2]$  for Mg or  $\dots[3s^2 3p^2]$  for Si) are photoionized by an external X-ray source (supposedly an XFEL beam) hereafter named as "the pump", tuned above the  $K$  edge. This pumping results in the population of the core-excited state  $|2\rangle$  radiatively coupled to state  $|1\rangle$  by the decay  $2p \rightarrow 1s$ . In conditions of weak pumping, this coupling corresponds to the usual  $K\alpha$  fluorescence. Note that in conditions of weak pumping, state  $|2\rangle$  predominantly decays via Auger decay (with the rate  $\Gamma_2$ ) while both states  $|1, 2\rangle$  are also affected by the photoionizing pump. We neglect here the fine-structure splitting of  $K\alpha$  line since it is smaller than the Auger width (this is true for Mg but more approximative for Si). Levels  $|1, 2\rangle$  are the two levels considered in our Bloch-Maxwell modeling. According to Fig. 1 and Fig. 2, quantities  $\gamma_1$ ,  $\gamma_2$  and  $X_p$  depend on the local intensity of the pump  $I_p$  in the sense that

$$\gamma_1(z, t) = \sigma_{1s} \frac{I_p(z, t)}{h\nu_p} \quad (17)$$

$$\gamma_2(z, t) = \Gamma_2 + \frac{\sigma_{1s}}{2} \frac{I_p(z, t)}{h\nu_p} \quad (18)$$

$$X_p(z, t) = \sigma_{1s} N_o(z, t) \frac{I_p(z, t)}{h\nu_p} \quad (19)$$

where  $\sigma_{1s}$  denote the  $1s$  photoionization cross-section at energy  $h\nu_p$ .  $I_p$ ,  $h\nu_p$  are the intensity (here a power per surface unit) and the photon energy of the pump, respectively.  $N_o$  is the population density of state  $|0\rangle$ . At this step it is important to remark that, for a normal incidence and being off an accidental situation where the period of the material would be an integer of  $\lambda/2$  (i.e. off-Bragg), one may adopt for the pump the simple *corpuscular* point of view of photon absorption. Hence, for a pump propagating from the right (see Fig. 2), the pump intensity obeys the following photon transport equation

$$\frac{1}{c} \frac{\partial I_p(z, t)}{\partial t} - \frac{\partial I_p(z, t)}{\partial z} = -k_p(z, t) I_p(z, t) \quad (20)$$

with

$$\begin{aligned}
k_p(z, t) &= \sigma_{1s} N_o(z, t) + \sigma_{1s} N_1(z, t) + \frac{\sigma_{1s}}{2} N_2(z, t) \quad (\text{in the active material}) \\
&= \sigma^{passive} N^{passive}(z, t) \quad (\text{in the passive material})
\end{aligned}$$

in which  $N^{passive}(z, t)$  is the atom density in a *passive* layer,  $\sigma^{passive}$  being the corresponding absorption cross section at  $h\nu_p$ . Finally, the population of state  $|0\rangle$  evolves as

$$\frac{\partial N_o(z, t)}{\partial t} = -\sigma_{1s} N_o(z, t) \frac{I_p(z, t)}{h\nu_p}. \quad (21)$$

In the case where the pump is explicitly taken into account, equations (17)-(21) have to be solved simultaneously with the previous Bloch-Maxwell set of equations.

In the following, we describe the propagation of an X-ray pulse at the  $K\alpha$  frequency for different situations of increasing complexity whether the pulse is of external origin or not (i.e. originating from spontaneous emission).

### A. Simple propagation in a multilayer material

A first and minimal implementation amounts to considering that all the layers are of *passive* nature, i.e. simply described by a complex refractive index. The goal is to assess the necessary number of subdivisions of each layer in our specific problem of wave propagation in the x-ray range, in a stratified medium made of nm-size layers. Indeed, this number of subdivisions defines a typical space interval  $\Delta z$  on which Maxwell equations are discretized according to the FDTD scheme mentioned above. Of course, this defines the time step  $\Delta t$  as discussed in Sec. II-B. As a test case, we consider here a sample already considered in a context of synchrotron irradiation [26]. It consists in a stack of 30 bilayers (Mg/Co) of thicknesses  $e_1 = 5.45$  nm and  $e_2 = 2.55$  nm, respectively so that the whole stack is denoted (Mg/Co)<sub>30</sub>. In each Mg layers, a source of radiation is supposed to emit at the  $K\alpha$  line energy (1253.6 eV). These sources are all the same. The resulting time-integrated outgoing emission over a time well exceeding both the time duration of the source and the time of propagation through the sample, is displayed in Fig. 3 as a function of the number of subdivisions in each layer. Specific modulations (called Kossel patterns) are observed at the Bragg angles of the multilayer. These modulations are due to interferences of the diffracted waves inside the material [27, 28]. Outgoing signals displayed in Fig. 3 are similar to the

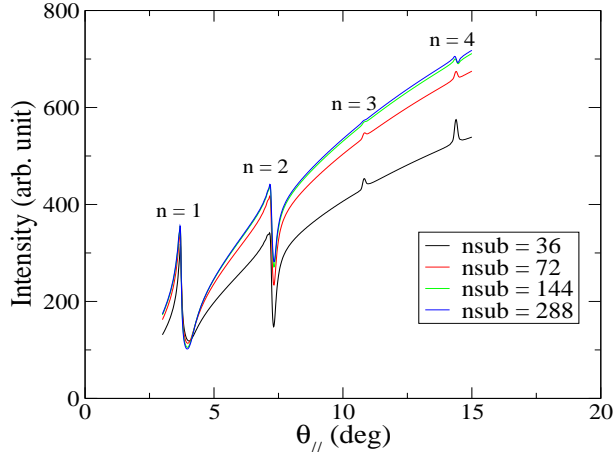


FIG. 3: (Color online) Calculated angular scan for the Mg  $K\alpha$  radiation emitted by a stack  $(\text{Mg}/\text{Co})_{30}$  ( $e_1 = 5.45$  nm and  $e_2 = 2.55$  nm) where a same source of  $K\alpha$  radiation has been put in each Mg layer. Kossel patterns are labelled by their Bragg order  $n$ .

ones calculated for the same sample but by solving the Helmholtz wave equation for a plane wave *incident* in the sample [14], which is just a check of the *optical reciprocity theorem* stated as *a point source at A will produce at B the same effect as a point of equal intensity placed at B will produce at A* [29, 30]. In Fig. 3, one sees a convergence in the number of subdivisions necessary for performing accurate calculations of x-ray pulse propagation in multilayered materials. It is interesting to note the extinction of Kossel structure  $n = 3$  for the converged results. This is consistent with the diffraction theory when applied to a simple line grating [30] or to X-UV interference mirrors [31]. Indeed, the first extinction should occur for the ratio  $\frac{\Lambda}{e_2} = 3$ . Taking for  $e_2$  and for the period  $\Lambda = e_1 + e_2$ , the values given above, one finds a value very close to 3. These different remarks validate our minimal implementation,

### B. Propagation in an amplifying multilayer material

We consider here the problem of a short pulse originating at the left, i.e. in the vacuum cell of our computational domain (see Sec. II-B) and then propagating from left to right in a multilayer similar to the stack considered in the previous paragraph, albeit with an increased number of bilayers, i.e.  $(\text{Mg}/\text{Co})_{60}$ . The Mg layers are now *active*, i.e. described by the Bloch equations, and we consider four typical sets of initial populations for  $N_1$ ,  $N_2$

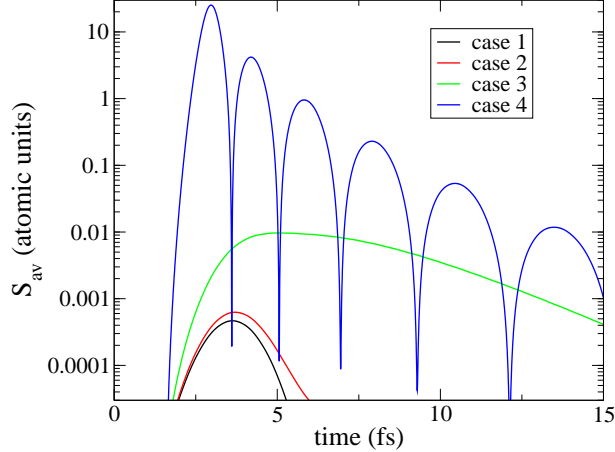


FIG. 4: (Color online) Modulus of the Poynting vector outgoing from the stack  $(\text{Mg}/\text{Co})_{60}$  in the normal direction ( $\theta_{//} = 90^\circ$ ), as a function of time. See text for the characteristics of the ingoing signal and for the definition of cases 1-4.

in term of the total density of atoms in solid state Mg that is  $n_{Mg} = 4.3063 \cdot 10^{22} \text{ cm}^{-3}$ . Population of the lowest level is fixed to  $N_1 = 4.306 \cdot 10^{18} \text{ cm}^{-3}$  while  $N_2$  is varied between  $4.306 \cdot 10^{17} \text{ cm}^{-3}$  (case 1),  $4.306 \cdot 10^{20} \text{ cm}^{-3}$  (case 2),  $4.306 \cdot 10^{21} \text{ cm}^{-3}$  (case 3),  $4.306 \cdot 10^{22} \text{ cm}^{-3}$  (case 4), respectively. In this way, case 1 corresponds to a very weak 1s photoionization with no inversion while case 4 corresponds to a maximal population inversion in the Mg layers. The ingoing pulse is of the form  $E(t) = \frac{1}{\sqrt{2\pi}\tau_p} \exp[-0.5(t - t_o)^2/\tau_p^2] \sin \omega_o t$  with the typical parameters  $\tau_p = 1 \text{ fs}$  and  $t_o = 2 \text{ fs}$ . What is specifically studied here is the right outgoing intensity as a function of time. More precisely, one displays the modulus of the Poynting vector, averaged over one period, i.e.  $S_{av} = \frac{1}{T} \int_0^T |S| dt$  with  $\mu_o^2 S^2 = (E_x B_z)^2 + (E_x B_y)^2$ ,  $B_z = \frac{1}{c} E_x \sin \theta_\perp$ . Hereafter, units for the Poynting vector are the atomic units, i.e.  $S_{av}$  is in unit of  $\frac{e^{12}}{(4\pi\epsilon_o)^6} \frac{m_e^4}{h^9}$ . For a signal ingoing in the normal direction, calculations are displayed in Fig. 4.

Compared with the weak signal (case 1), one sees the gradual effect of a gain material on the intensity temporal shape of the outgoing pulse. In particular, one notices an increase of the outgoing pulse duration with respect to the ingoing pulse duration. In the case of strong (and here maximal) inversion (case 4), a typical effect such as "ringing" of the outgoing signal is observed. This correspond to the well-known Burnham-Chiao ringing [32]. Present simulations are in the time domain. Of course, taking the Fourier transform

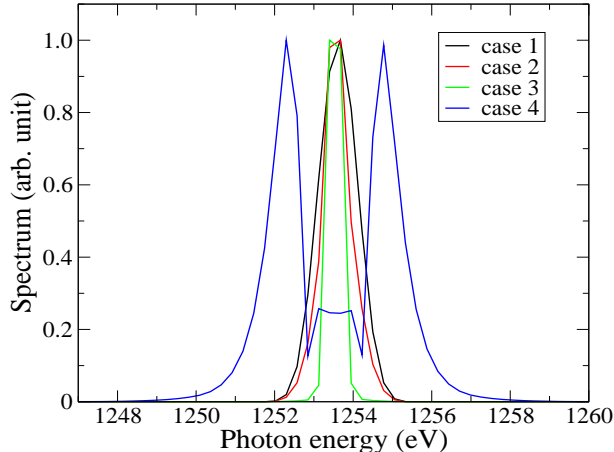


FIG. 5: (Color online) Normalized spectra corresponding to the signals of Figure 4.

gives information on the frequency domain. Fig. 5 shows the spectra corresponding to the previous simulations, i.e. the evolution of the (normalized) spectrum as a function of the density of inversion. Even on this small distance of propagation, the high density allows a clear gain narrowing (case 2 and case 3) and then a strong AC Stark (or Rabi) splitting for the maximal density of inversion (case 4). This behavior illustrates the response of the two-level system driven by an x-ray field on resonance. This field becomes so important that the levels shift dynamically through the Stark effect.

### C. Self-emission of an amplifying multilayer material

In this paragraph, we do not consider the propagation of an external pulse but the signal originating from the noisy source of spontaneous emission in each active cell of a multilayer. More precisely, we study how spontaneous emission emitted in one direction propagates and how stimulated emission sets in. Present calculations rely on the modeling of spontaneous emission presented in Sec. II-C. Still for the same multilayer  $(\text{Mg}/\text{Co})_{60}$  and the same sets of initial populations  $(N_1, N_2)$  in Mg layers, Fig. 6 displays simulations of the outgoing X-ray emission in the normal direction.

We see the weak noisy signal for a low initial excitation (case 1) while, gradually with the density of inversion, a collective emission is set up independently of any external pulse ingoing into the material. For the maximal initial population inversion (case 4), characteristics of the superradiance, namely time delay for the peak of emission and ringing are clearly visible.

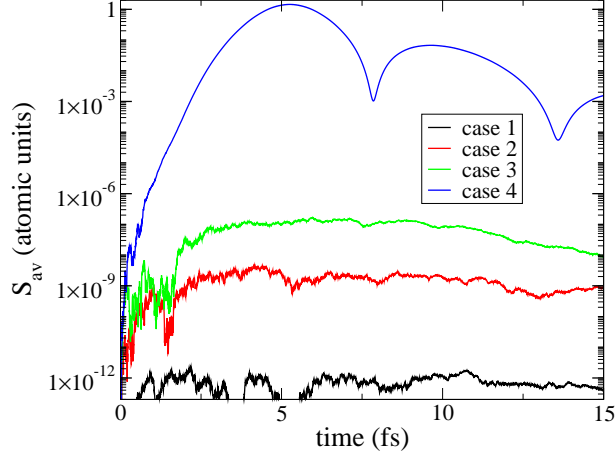


FIG. 6: (Color online) Modulus of the Poynting vector outgoing from the stack  $(\text{Mg/Co})_{60}$  in the normal direction ( $\theta_{//} = 90^\circ$ ), as a function of time. The seeding is provided by the inherent spontaneous emission noise. See text for the for the definition of cases 1-4.

We turn now to a propagation seeded around the first uncorrected Bragg angle (defined so that  $\Lambda \sin \theta_{//} = \lambda/2$ ,  $\Lambda$  being the period of the material, i.e.  $\Lambda = e_1 + e_2$  according to Fig. 2). Here an oscillation feedback can be provided by Bragg reflection [12, 13, 33] so that large electric field enhancements can be obtained [14]. Note that, for a multilayer and in the linear response regime, a small deviation to the previous Bragg law exists [34, 35]. Compared with Fig. 6 (normal direction), a dramatic change of the emission is observed for  $\theta_{//} = 3.45^\circ$ . Here at oblique incidence, the phase front of a plane wave incident on the left is supposed to arrive on the opposite side in a very short time. This time  $\tau$  is defined so that  $c\tau = d \sin \theta_{//}$ ,  $d$  being the whole thickness of the multilayer, i.e.  $\tau \simeq 0.1 \text{ fs}$  in present conditions. As one can see, depending on the inversion density, the outgoing x-ray pulse shifts earlier in time, its duration is reduced while its intensity strongly increases. This is a clear evidence of the feedback provided by Bragg reflection in the multilayer. Some complex "ringing" is also apparent. The corresponding spectra are shown in Fig. 8. The huge broadening observed for the maximal density of inversion (case 4) is a combined effect of the pulse shortening and of AC Stark splitting due to the huge electric field which sets up. These results suggest that for large population inversions, emission will tend to be around the Bragg angle and that its duration should be extremely short, beating even Auger decay which is of the order of 2-3 fs.

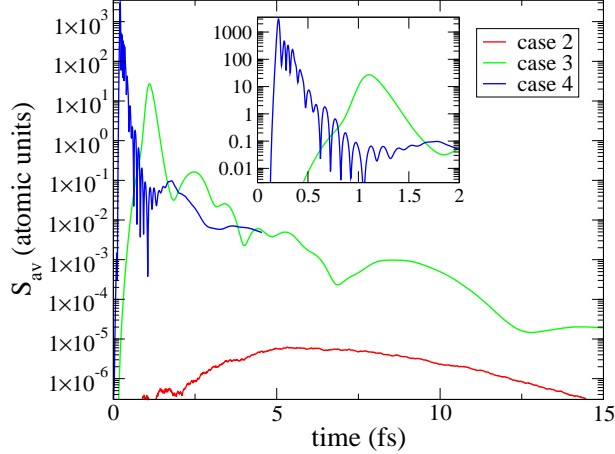


FIG. 7: (Color online) Modulus of the Poynting vector outgoing from the stack  $(\text{Mg}/\text{Co})_{60}$  in first Bragg direction  $\theta = 3.45$  deg, as a function of time. The seeding is provided by the inherent spontaneous emission noise. See text for the for the definition of cases 2-4. The inset is a zoom of the time interval 0-2 fs.

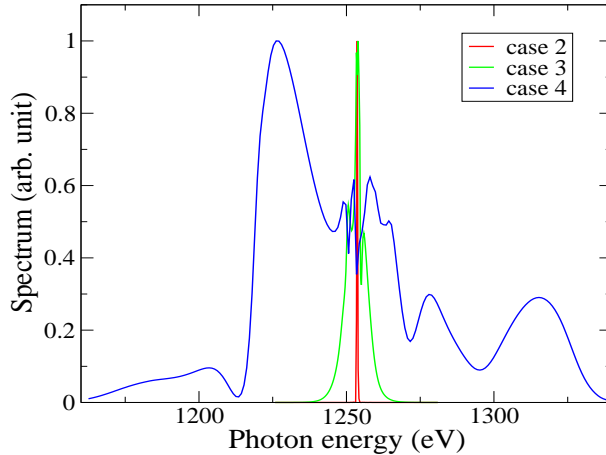


FIG. 8: (Color online) Normalized spectra corresponding to the signals of Figure 7.

#### D. Self-emission of a pumped multilayer material

Previous calculations were based on the idea of a preliminary preparation of  $N_1$ ,  $N_2$  at given initial values. Here we place ourselves in conditions where these initial values are zero and where pumping of level 2 is provided by an external x-ray source photoionizing the ground level (of population  $N_0$ ) within an active layer, as discussed at the beginning of

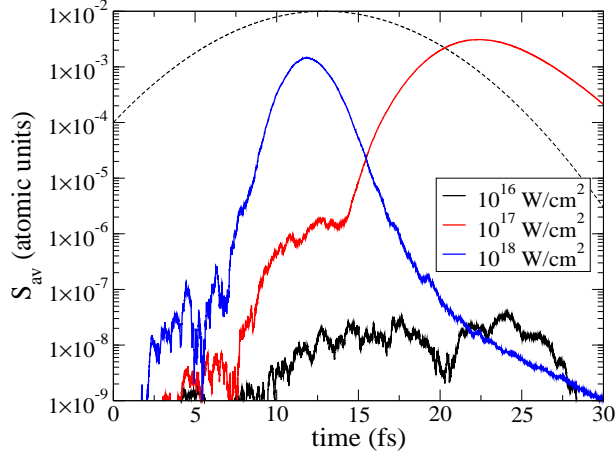


FIG. 9: (Color online) Modulus of the Poynting vector outgoing from the stack  $(\text{Mg}/\text{Co})_{60}$  in the normal direction ( $\theta_{//} = 90^\circ$ ), as a function of time and for different intensities of an external X-ray pump. Dashes (of arbitrary unit) indicate the temporal shape of the pump. The seeding of the emission is provided by the inherent spontaneous emission noise.

Sec. III. In present simulations, the x-ray pulse is supposed Gaussian and of 10 fs duration (FWHM). The photon energy of this pump is 1332 eV, i.e. above the Mg K-edge. In Fig. 9, we plot the outgoing Mg  $K\alpha$  emission of our  $(\text{Mg}/\text{Co})_{60}$  stack in the normal direction, as resulting from three different pump intensities. Pump irradiation is at normal incidence, i.e. according to Fig. 2. Its intensity is propagated and depleted according to Eq. (20). Dashes (of arbitrary unit) indicate the temporal shape of the pump. Here, the different shapes of the outgoing emission reflect the efficiency of the core-hole creation with respect to the maximum of intensity. As seen above, the signal stops to be noisy when stimulated emission sets up which is possible if a sufficient density of core-holes is reached. Now, as expected from the considerations of Sec. III-C, the signals observed in the Bragg direction  $\theta_{//} = 3.45^\circ$ , are dramatically different (Fig. 10) both in intensity (few orders of magnitudes) and in temporal shape. The complex behavior of outgoing signals reflects the complex interplay between population kinetics, depletion of the pump, propagation and Bragg diffraction. This is somehow illustrated by snapshots of the spatial distribution (inside the multilayer) of populations  $N_0$ ,  $N_1$ ,  $N_2$  at different characteristic times during the driving pump pulse (Fig. 11). The x-ray pump comes on the right so that the decrease of population  $N_0$  as a function of  $z$  reflects the attenuation of the pump as it propagates from the right to the left inside the material. The Bloch-Maxwell coupling of populations  $N_2$ ,  $N_1$ , seeded by

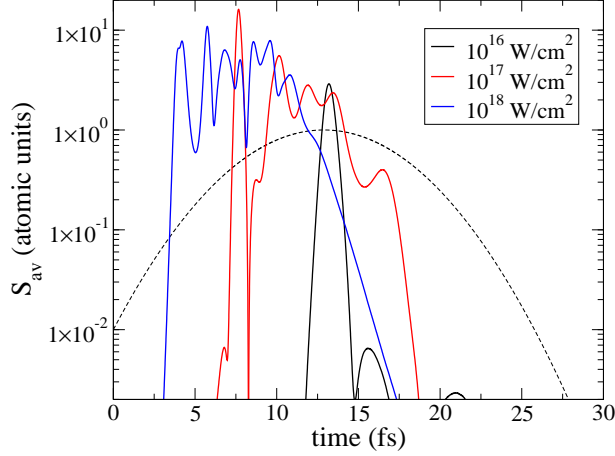


FIG. 10: (Color online) Modulus of the Poynting vector outgoing from the stack  $(\text{Mg}/\text{Co})_{60}$  in the direction  $\theta_{//} = 3.45^\circ$ , as a function of time and for different intensities of the external X-ray pump. Dashes (of arbitrary unit) indicate the temporal shape of the pump. The seeding of the emission is provided by the inherent spontaneous emission noise.

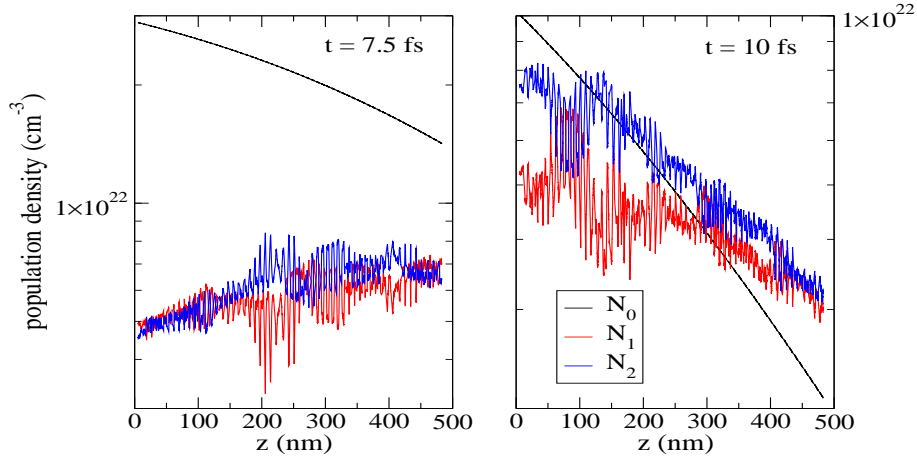


FIG. 11: (Color online) Snapshots of populations  $N_0$ ,  $N_1$ ,  $N_2$  at 2 moments inside the multilayer  $(\text{Mg}/\text{Co})_{60}$  and in the conditions of Fig. 10. The pump comes on the right with an intensity of  $10^{18} \text{ W}/\text{cm}^2$ . Left figure:  $t = 7.5 \text{ fs}$ ; right figure  $t = 10 \text{ fs}$ .

spontaneous emission, gives rise to a set of pulses propagating inside the multilayer and to clear Rabi oscillations (Rabi flopping). Despite the complex temporal shape of these outgoing signals around the Bragg direction, they remain much more intense than in the normal direction.

### E. Self-emission of a pumped natural crystal

In this last section, one examines the case of a natural crystal whose periodicity of atomic layers may provide the same kind of Bragg oscillations. One considers here a Si crystal where for an orientation (110) of planes parallel to the surface, atomic layer spacing is  $d = 0.385$  nm. A strong pumping of 1s core electrons in Si may give rise to an amplification on the  $2p \rightarrow 1s$   $K\alpha$  line at 1740 eV. At this energy the first Bragg angle is around  $67.7^\circ$  (with respect to the surface). 1D Periodicity is introduced in the calculations by considering the (supposedly perfect) crystal as a stack of bilayers of period  $d$  and where the first layer (the active layer) is a layer of Si atoms while the second layer is just empty (then passive) and of refractive index 1. The thickness of the Si layers corresponds to the size of Si atoms, i.e. to  $0.34 \times d$ . Simulations presented here correspond to a Si thickness of  $1.92 \mu\text{m}$ , i.e. to the stack  $(\text{Si}/\text{vacuum})_{5000}$ . To optimize the homogeneity of the pumping, i.e. to limit the pump depletion along the  $z$  axis (referring to Fig. 2) it is somewhat interesting to change the irradiation axis by choosing the  $y$  axis as irradiation axis. In this way, assuming a small quantity of matter along the  $y$  axis (typically less one  $\mu\text{m}$ ) preserves the 1D geometry of the problem. Simulation results are displayed in Fig. 12. Irradiation conditions are a Gaussian pulse of 10 fs duration (FWHM), 1900 eV of photon energy (i.e. above the Si K-edge) and of intensities  $10^{17}$  W/cm<sup>2</sup>. Fig. 12 displays a comparison of the outgoing Si  $K\alpha$  signal (i.e. seeded by spontaneous emission) observed in the normal direction  $\theta_{//} = 90^\circ$ , in the Bragg direction  $\theta_{//} = 67.75^\circ$  and in some off-Bragg direction, respectively. Compared with the other directions, emission in the Bragg diffraction region (the Kossel region) is clearly enhanced which indicates the possibility of having a resonator or feedback effect in a natural crystal.

## IV. CONCLUSION

A 1D Bloch-Maxwell FDTD model for any oblique incidence has been successfully implemented for studying x-ray propagation in 1D photonic crystals. We simulated the self-emitted signal from typical 1D photonic crystals where a population inversion is prepared on an atomic transition in the x-ray range. The build up of outgoing signal starts from spontaneous emission. We have seen that this emission encompasses many non-linear phe-

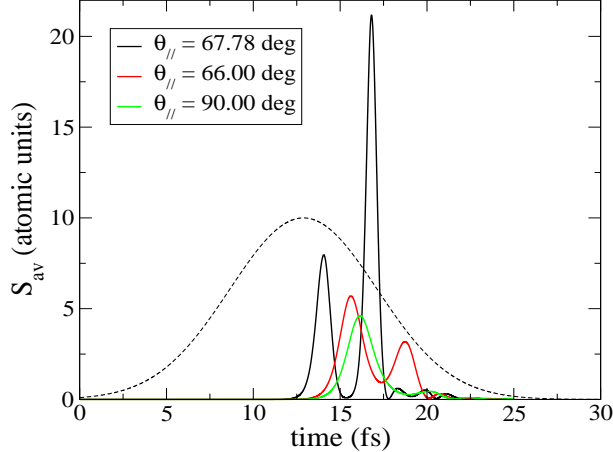


FIG. 12: (Color online) Modulus of the Poynting vector outgoing from the stack  $(\text{Si}/\text{vacuum})_{5000}$  ( $e_1 = 0.1309$  nm,  $e_2 = 0.2541$  nm) irradiated in the transverse direction by a Gaussian pulse of intensity  $10^{17}$  W/cm<sup>2</sup>, 10 fs duration, 1900 eV photon energy. Dashes (of arbitrary unit) indicate the temporal shape of the pump. Three outgoing directions are shown: the normal direction  $\theta_{//} = 90^\circ$ , the Bragg direction  $\theta_{//} = 67.78^\circ$  and an off-Bragg axis direction  $\theta_{//} = 66.0^\circ$ . Seeding of the emission is provided by the inherent spontaneous emission noise.

phenomena such as Rabi splitting, Rabi flopping, ringing, etc in the x-ray range as well as the Kossel effect but in an *amplified mode*. We have shown that most of the emission occurs in a prevailing direction which is the Bragg direction. If the inversion results from a previous photoionization, we observed that this emission is short enough to beat Auger relaxation. We specifically studied cases where the pumping source allowing a strong population inversion is an intense, short x-ray pulse such as provided by XFEL sources. For a typical multilayer and for realistic conditions of pumping, calculations show a strong enhancement of the emission in the Bragg direction. For the case of natural crystals, this enhancement is also noticeable.

Results of this study motivate future experimental investigations of the behavior of photonic crystals whether they are natural or artificial (multilayers). It motivates also many other theoretical investigations on different multilayers or natural crystals to optimize x-ray emission at different wavelengths.

## **Acknowledgments**

At numerous times during the course of this work, one of us (O. Peyrusse) has benefited from discussions and helpful advices concerning the use of computational resources from Paul Genesio at PIIM laboratory.

- 
- [1] B.W. Adams et al., *J. Mod. Opt.* **60**, 2 (2013).
- [2] B.W. Adams, *Nonlinear Optics, Quantum Optics and Ultrafast Phenomena with X-rays* (Kluwer Academic Publisher, Norwell, MA, 2008).
- [3] Yu-Ping Sun et al., *Phys. Rev. A* **81**, 013812 (2020).
- [4] N. Rohringer et al., *Nature* **481**, 488 (2012).
- [5] A. Benediktovitch et al., *Phys. Rev. A* **101**, 063412 (2020).
- [6] M. Beye et al., *Nature* **501**, 191 (2013).
- [7] H. Yoneda et al., *Nature* **524**, 446 (2015).
- [8] P. Jonnard et al., *Struct. Dyn.* **4**, 054306 (2017).
- [9] T. Kroll et al., *Phys. Rev. Lett.* **120**, 133203 (2018).
- [10] A. Halavanau et al., *P.N.A.S.* **117**, 15511 (2020).
- [11] M. Nagasono et al., *Phys. Rev. Lett.* **107**, 193603 (2011).
- [12] A. Yariv and P. Yeh, *Optics Comm.* **22**, 5 (1977).
- [13] J.-M. André, K. Le Guen, and P. Jonnard, *Laser Phys.* **24**, 085001 (2014).
- [14] O. Peyrusse et al., *Phys. Rev. A* **101**, 013818 (2020).
- [15] J.C. MacGillivray and M.S. Feld, *Phys. Rev. A* **14**, 1169 (1976).
- [16] O. Larroche et al., *Phys. Rev. A* **62**, 043815 (2000).
- [17] C. Weninger and N. Rohringer, *Phys. Rev. E* **90**, 063828 (2014).
- [18] C. Lyu, S.M. Cavaletto, C.H. Keitel, et al., *Sci. Rep.* **10**, 9439 (2020).
- [19] A. Taflove, *Computational Electrodynamics. The Finite-Difference Time-Domain Method* (Artech House, 1995).
- [20] B.L. Henke, E.M. Gullikson, and J.C. Davis, *At. Data. Nucl. Data Tables* **54**, 181 (1993).
- [21] CXRO <http://www.cxro.lbl.gov/>.
- [22] M.O. Scully and M.S. Zubairy, *Quantum optics* (Cambridge University Press, Cambridge, England, 1997).
- [23] K.S. Yee, *IEEE Trans. Antennas Propag.* **14**, 302 (1966).
- [24] B. Engquist and A. Majda, *Math. Comput.* **31**, 629 (1977).
- [25] D.E. Merewether, R. Fisher, and F.W. Smith, *IEEE Trans. Nucl. Sc.* **27**, 1829 (1980).
- [26] P. Jonnard et al., *J. Phys. B* **47**, 165601 (2014).

- [27] E. Langer and S. Däbritz, IOP Conf. Series: Materials Science and Engineering **7**, 012015 (2010).
- [28] K. Le Guen et al., J. Nanosci. Nanotechnol. **19**, 593 (2019).
- [29] W. Schülke and D. Brümmer, Z. Naturforsch. Teil A **17**, 208 (1962).
- [30] M. Born and E. Wolf, *Principles of Optics, Sixth Edition* (Pergamon Press, 1980).
- [31] B. Pardo, T. Megademini, and J.M. André, Revue Phys. Appl. **23**, 1579 (1988).
- [32] D.C. Burnham and R.Y. Chiao, Phys. Rev. **188**, 667 (1969).
- [33] A. Yariv, Appl. Phys. Lett. **25**, 105 (1974).
- [34] D. Attwood, *Soft X-rays and Extreme Ultraviolet Radiation* (University of California, Berkeley, 2007).
- [35] C.T. Chantler and R.D. Deslattes, Rev. Sci. Instrum. **66**, 5123 (1995).